Structure, Vol. 10, 1205–1210, September, 2002, ©2002 Elsevier Science Ltd. All rights reserved. PII S0969-2126(02)00830-4

Trichromatic Concept Optimizes MAD Experiments in Synchrotron X-Ray Crystallography

Takashi Kumasaka,[1,2] Masaki Yamamoto,[1,5] Eiki Yamashita,[3] Hideaki Moriyama,[4] and Tatzuo Ueki[4]

[1]X-Ray Coherent Optics Laboratory
RIKEN Harima Institute/SPring-8
Mikazuki, Sayo
Hyogo 679-5148
Japan

[2]Department of Life Science
Tokyo Institute of Technology
Nagatsuta-cho, Midori-ku
Yokohama 226-8501
Japan

[3]Institute for Protein Research
Osaka University
Yamadaoka, Suita
Osaka 565-0871
Japan

[4]The Japan Synchrotron Radiation Research Institute (JASRI)/SPring-8
Mikazuki, Sayo
Hyogo 679-5198
Japan

Summary

The trichromatic concept is a new synchrotron beamline design that optimizes MAD experiments by reducing systematic experimental errors with three-colored and coaxial synchrotron X-ray beams produced by a tandem vertical undulator and trichromator. The concept enables rapid and flexible switching of three defined wavelengths, and extends the flexibility of experimental design for MAD data collection. Thus, we can collect MAD data taking into account time series effects such as radiation damage. The data based on the trichromatic concept gave a better quality electron density map than data collected by conventional methods. It was also revealed that multicolor diffraction using dichromatic or trichromatic X-ray beams is effective in rapid MAD data collection.

Introduction

The trichromatic concept is a new design of synchrotron beamline meant to optimize the multiwavelength anomalous diffraction (MAD) method using highly brilliant and energy-tunable synchrotron radiation [1]. Nowadays, the MAD method is widely used for crystallographic determinations of unknown protein structures [2–4], since the scope of MAD application has been extended by the use of synchrotron radiation facilities, the biological technique for the production of selenomethionyl protein [5], and computational development. The method requires only one crystal containing anomalous scattering atoms. This contributes to the improvement of throughput in crystal structure determination. However, it is essential for more precise diffraction data sets to reduce systematic experimental error due to absorption effect, crystal degradation, and the quality of incident X-ray, since the method depends on weak anomalous signals by Bijvoet and dispersive differences.

Most protein crystals suffer from radiation damage. The radiation damage depends on the amount of radiation dose, and will decay the data quality in time with irreversible and unpredictable crystal degradation [6]. Although the cryocrystallographic technique is effective in reducing the degradation, radiation damage has often been observed [6, 7]. Even for such radiation-sensitive crystals, several data sets of multiple wavelengths have to be collected from only one crystal using highly brilliant synchrotron radiation in MAD experiments. These effects make the diffraction intensities of protein crystals vary during the data collection. As a result, the agreement factor among data (such as R_{iso} and R_{sym}) would be degenerated, and it would be difficult to obtain true anomalous signals.

In principle, the Bijvoet and dispersive differences would be recorded in different crystal orientations and different incident X-ray wavelengths, respectively. In other words, the Bijvoet difference is recorded in a single data set, while the dispersive difference can be extracted as differences between two individual data sets. Thus, the degrees of agreement in a single data set and among data sets affect the quality of MAD phases. Here we assume that the disagreements between Bijvoet- and dispersive-related intensities are described as the sum of two components: anomalous terms and time-dependent shift of intensities (time lag error). The latter is caused by unpredictable structural degradation in crystals. In this case, the problem is how to reduce the time lag error, and can be solved by considering data collection scheduling. The inverse beam geometry technique is often used to improve the agreement of Bijvoet-related reflections in single-wavelength data. The technique is based on the fact that each Bijvoet (Friedel) mate is related to the inverse of 180° in the oscillation axis, and can be recorded serially only by the rotation of the axis. The mates are recorded under similar radiation conditions at the nearest scene in the time course of crystal degradation, and contain equal values of the time-dependent factor. Thus, the time lag error will vanish in the Bijvoet difference. On the other hand, the treatment for the dispersive term has been technically difficult since it requires rapid wavelength switching, with rapid tuning and good reproducibility of X-ray optical devices.

The trichromatic concept was designed with consideration of these aspects in MAD experiments and realized at the RIKEN beamline I (BL45XU) at the third generation synchrotron facility, SPring-8 (Harima, Hyogo, Japan). It has been successfully applied to many crys-

[5]Correspondence: yamamoto@postman.riken.go.jp

Key words: MAD; synchrotron radiation; trichromatic concept

A

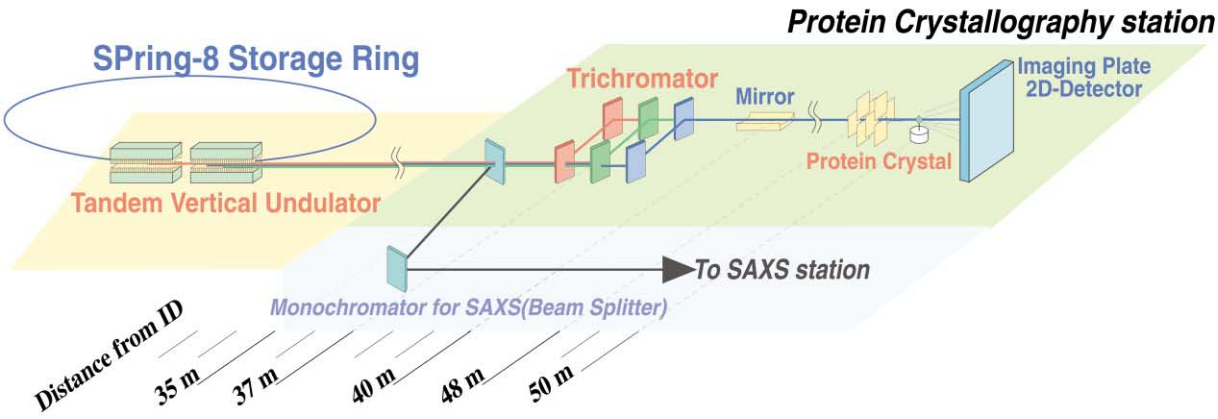

B

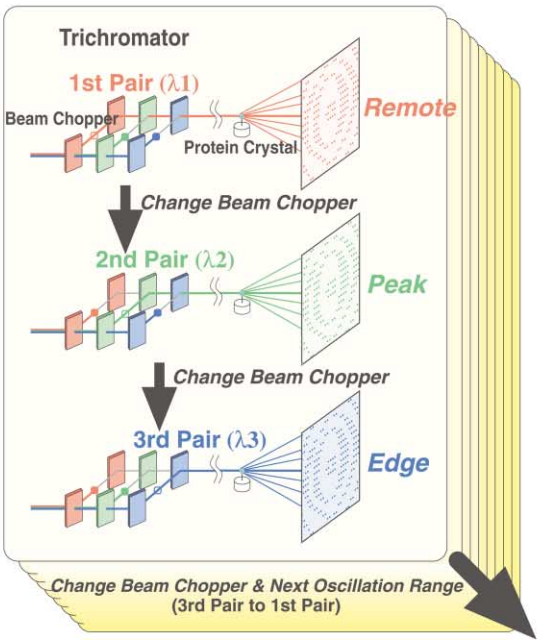

Figure 1. Schematic Drawing of RIKEN Beamline I and the Trichromatic Concept

(A) Beamline assembly. Two vertical undulators are arranged serially and are called the tandem vertical undulator. The trichromator consists of three pairs of diamond double-crystal monochromators, and provides the three monochromatized X-ray beams coaxial with each of three wavelengths (λ_1, λ_2, and λ_3) at the same time.

(B) MAD data collection with the trichromatic concept. Three diffraction patterns from three different wavelength X-rays are recorded sequentially with the same oscillation angle for an identical crystal using the trichromator with the beam choppers. By combining the vertical tandem undulator, the beamline covers the energy range of 7.5–14.0 keV (0.89–1.65 Å).

tals with various anomalous scatterers. These results show that the trichromatic concept is powerful and effective for MAD analyses. We describe here the trichromatic concept, the beamline, and the MAD analyses.

Trichromatic Concept and Beamline

To promote advanced experiments by the MAD method, we have proposed the trichromatic concept [8]. This concept is composed of three aspects: (1) high-brilliance (low-divergence) beams of different energies from two successive undulators, (2) high-energy resolution from monochromator crystals made of synthetic diamond, and (3) a rapid switching incident wavelength using a transparent monochromator for care of the dispersive term.

The trichromatic concept takes maximum advantage of the third generation synchrotron, especially the efficiency of undulators. The undulator is a synchrotron

Table 1. Data Collection and Phasing Statistics of a ChoA Crystal

Data	Cho1 (trichromatic method)			Cho2 (conventional method)		
	Cho11	Cho12	Cho13	Cho21	Cho22	Cho23
Wavelength (Å)	1.02000 (remote)	0.97905 (peak)	0.97960 (inflection)	1.02000 (remote)	0.97905 (peak)	0.97960 (inflection)
Observation	260,402	269,821	269,362	261,577	263,567	263,387
Individuals	65,579	66,482	66,428	65,695	66,480	66,499
Completeness[a] (%)	97.6 (86.1)	99.0 (98.3)	99.0 (98.3)	97.6 (86.4)	98.8 (98.1)	98.8 (98.2)
R_{merge}[a] (%)	4.9 (18.3)	5.3 (22.9)	8.4 (27.7)	4.5 (16.5)	4.8 (20.1)	7.6 (29.7)
I/σ_I	18.5	17.4	17.5	19.8	18.7	17.1
R_{iso} with remote[a] (%)		5.7 (9.8)	4.8 (9.4)		6.4 (10.0)	7.1 (11.5)
R_{iso} with peak[a] (%)			3.2 (8.4)			4.0 (9.1)
Isomorphous rms (ϵ)[b] (acentric/centric)		8.1/12.5	8.9/14.0		10.3/16.8	8.9/14.7
Anomalous rms (ϵ)[b]	7.32	16.56	8.98	6.37	15.91	8.11
Isomorphous R_{Cullis}[c] (acentric/centric)		0.83/0.88	0.82/0.84		0.78/0.86	0.78/0.83
Anomalous R_{Cullis}[c]	0.99	0.91	0.94	0.99	0.91	0.93
Mean figure of merit	0.4508			0.4887		
Phasing power[d] (acentric/centric)	1.82/—	1.19/0.82	1.22/0.81	1.85/—	1.38/0.89	1.40/0.90
f'/f''[e]	−3.22/0.57	−8.01/8.67	−9.63/2.54	−1.73/0.54	−9.92/10.57	−9.27/2.13
$<\lvert\Delta\phi\rvert>$[f] (°)	44.2 (33.9)			47.8 (39.4)		

[a] The numbers in parentheses are for the outermost shell (1.80–1.70 Å).
[b] Weighted root-mean-square lack of closure: $\epsilon = |F_{PHi} - |F_P \exp(\phi_P) + F_H||$
[c] $R_{Cullis} = \text{rms}(\epsilon)/<|F_{PHi} - F_P|>$
[d] $<|F_H|/\epsilon>$
[e] Estimated by SOLVE.
[f] Phase difference with refined model. The models were refined with corresponding diffraction data. Phase differences between the models were within approximately 3°. The numbers in parentheses are for the resolution range of 10–2.5 Å.

X-ray source composed of two arrays of facing permanent magnets, and the emission from it is very brilliant and highly collimated. However, the tuning of emission energy is accompanied by the shift of the magnetic array gap, and the configuration of optical devices must generally be realigned. To lessen these time-consuming processes and to make preparations for all required incident wavelengths in advance, we constructed the new concept trichromator accompanied by the development of synthetic diamond crystals for higher transparency and higher energy resolution of incident X-rays.

The RIKEN beamline I at the SPring-8 is schematically illustrated in Figure 1A. In order to provide X-ray beams with three different energies, we installed two serially arranged, vertically polarized undulators, which are called tandem vertical undulators [9]. Each undulator is designed to emit radiation of photon energies from 6 to 14 keV as a fundamental harmonic, and is controlled independently through this energy range. Thus, the undulator beam, which has two energy peaks, is introduced to the trichromator. The trichromator [8, 10] consists of three pairs of transparent diamond monochromators, and brings out a "trichromatized" X-ray beam of three different wavelengths (λ_1, λ_2, and λ_3) at once. The switching and combining of any three wavelengths can be achieved in a few seconds by the rotation of the beam choppers located between two diamond crystals of individual monochromators. Thus, diffraction patterns of protein crystal from three different X-ray wavelengths can be successively exposed. Each monochromator crystal of the trichromator is made from synthetic diamond with the thickness of less than 0.3 mm and transmits about 70% of the incident beam at the wavelength of 1 Å (12.4 keV). By using the highly collimated undulator beam and the 4 0 0 reflection of the diamond crystal, high-energy resolution ($\Delta E/E = 3 \times 10^{-5}$) can be achieved, and the energy range covers from 7.5 to 14.0 keV (0.89–1.65 Å). The energy resolution is much better than that from the coupling of a bending magnet source and conventional Si (1 1 1) monochromator, and thus is more effective for anomalous measurement. The cylindrical bent mirror was installed next to the trichromator, and removes higher order harmonics and collimates the beams. The optimized beams finally reach the sample crystal position, which is placed 50 m from the undulator. The focusing size of the beam is less than 0.15×0.15 mm^2 and the total flux is estimated at over $3–4 \times 10^{11}$ photons/s at the sample position. The diffraction from sample crystals can be recorded on either a CCD detector or a fast readout imaging plate detector [11].

Since the trichromator can produce three colored and coaxial beams, a multiwavelength diffraction pattern could be recorded on a single oscillation image with dichromatic or trichromatic X-ray incident beams at once. The Bragg reflections can be recorded separately by using two distant wavelengths such as remote and inflection in MAD experiments, although they mostly overlapped each other at closer wavelengths. In this case, the total experimental time would be reduced to two-thirds. This is also advantageous for scaling and phasing in MAD calculation.

Results and Discussion

The statistics of ChoA data clearly show that the trichromatic concept optimizes MAD experiments and espe-

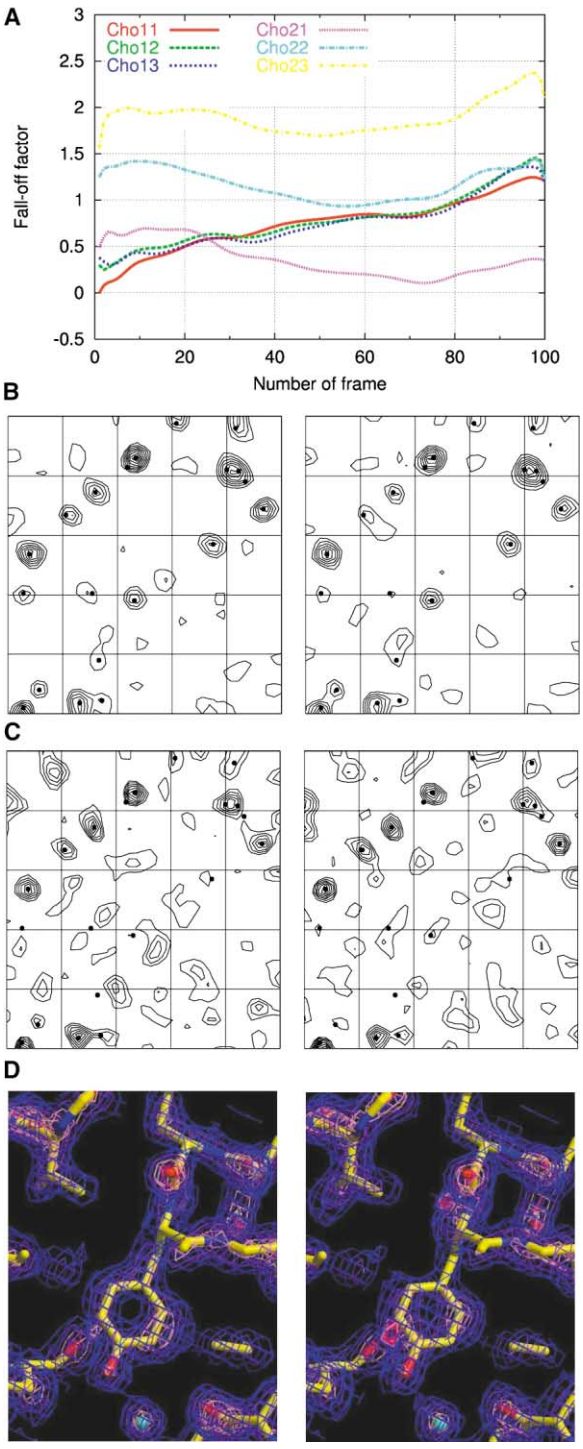

Figure 2. MAD Analyses of a ChoA Crystal

(A) Evaluated fall-off factors of ChoA diffraction images. The first image of Cho11 data was assigned as reference ($B = 0$). Each line is a Bezier curve fitted for the frame factors of each data set.

(B–D) Dispersive Patterson (B), Bijvoet Patterson (C), and MAD-phased Fourier (D) maps calculated from ChoA MAD data sets. The maps were contoured from 1 σ with 1 σ step. The left and right maps were calculated from trichromatic (Cho1) and conventional (Cho2) data sets, respectively. Patterson maps were prepared in the following manner: all reflections of less than 3 σ were excluded from the calculation. Solid circles indicate Patterson vectors of selenium sites. The coefficients were used as differences between remote and inflection data, and peak anomalous data, respectively. The maps show a Harker section at $w = 1/2$ and its u and v origins are located in the upper left corner. The u and v axes correspond to the across and down directions, respectively. The MAD Fourier maps at 1.7 Å resolution were prepared in the following manner: the coefficients and phases were solely calculated by CCP4 (MLPHARE) [13] without any phase modification. The maps show surroundings of Tyr165 of the ChoA A chain. The pictures were drawn by XtalView/Xfit [27] and Raster3D [28].

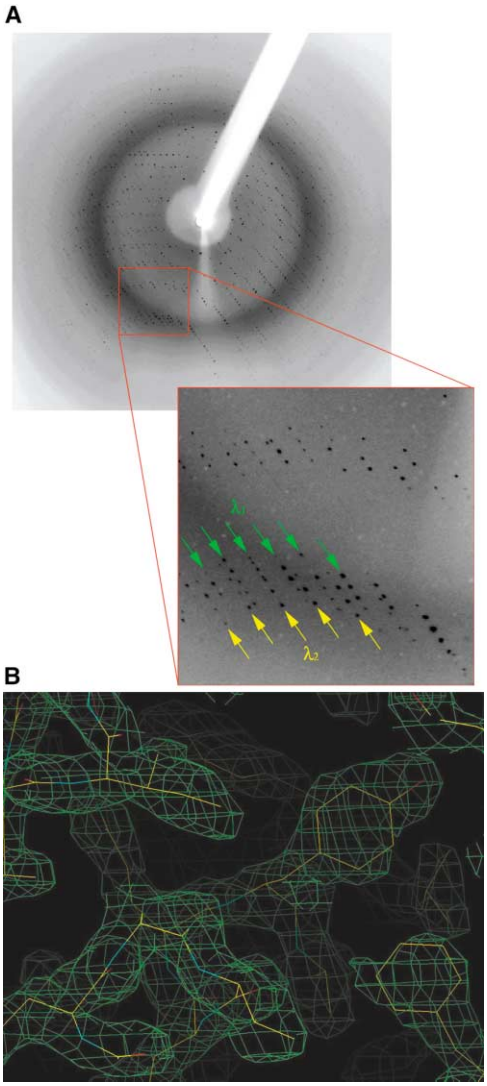

Figure 3. Dichromatic Diffraction Analysis of CA

(A) Dichromatic diffraction image. Arrows designated with λ_1 and λ_2 indicate the array of the reflections from remote and inflection wavelengths, respectively.

(B) MAD Fourier map. The map was calculated from MAD phase with solvent flattening and noncrystallographic symmetry averaging by CCP4 (DM) [13] and contoured at 1.5 σ. The picture was drawn by Turbo Frodo [29].

cially the measurement of dispersive terms (Table 1). The isomorphous R factor of the trichromatic data is smaller than that of conventional data. The graph of the

fall-off factors shows a critical difference between the two data collection methods (Figure 2A). In the trichromatic data, the fall-off factors of the same oscillation angles had almost the same values. On the contrary, the conventional data gave different values depending on the time series. The qualities of the individual data were almost the same, or rather the trichromatic data were slightly worse, than the conventional data in I/σ and the merging R factor.

The statistics of the agreement among the data sets showed that the trichromatic data are better than the conventional data. This trend was also observed in another trichromatic data set, which was collected with the crystal position identical to Cho2 after Cho2 data collection had been completed (data not shown). Anomalous difference Patterson maps from each data set showed distinguished features between the trichromatic and conventional experiments. Bijvoet difference Patterson maps showed consistent patterns (Figure 2C), however dispersive difference Patterson maps from the trichromatic data had higher peaks at reasonable positions (Figure 2B). This result showed that the signal-to-noise ratio in dispersive difference Patterson maps could be improved by the trichromatic method. The ChoA monomer has seven methionine residues, and its crystals contain two monomers per asymmetric unit. In any combination of data, the program SOLVE [12] could automatically find twelve selenium sites with the exception of the N terminus of each monomer, which could not be found in $2F_o-F_c$ maps at the current status of refinement.

Further advantages of the trichromatic data were also observed in phase calculations by CCP4 (MLPHARE) [13] with heavy atom parameters obtained from the refined model. The statistics based on isomorphous (dispersive) difference such as lack of closure and the Cullis R factor of the trichromatic data were better than those of the conventional data (Table 1). However, the statistics of the Bijvoet difference were better in the conventional data. The trichromatic concept does not obstruct the use of the inverse beam geometry technique, and the techniques could be applied together if needed to improve further agreement of the data. The contribution of two anomalous terms in phase determination depends on the magnitudes and accuracies of the terms, and thus both final mean figures of merit resulted in almost the same values. However, the mean phase difference and map correlation between MAD phase and true phase (calculated from the refined models) were better in the trichromatic data. Better mean phase errors result in a better electron density map. In particular, the electron densities for almost all six-membered rings are clearly observed as open circles from trichromatic data at 1.7 Å MAD phase (Figure 2D). These facts prove that the trichromatic concept is quite effective for MAD phasing.

Dichromatic data collection has been successfully applied to the structure determination of β-carbonic anhydrase (CA). A diffraction image shown in Figure 3A was taken with the X-ray beam including remote and inflection wavelengths. Most of the reflections are separated and could be processed by conventional densitometry software (such as HKL suite), whereas some of reflections show severe overlap. For these reasons, the statistics of the dichromatic data were worse than those of the monochromatic data (R_{merge} and $I/\sigma_I = 7.1\%$ and 16.4 in remote, 7.7% and 12.5 in peak, and 12.8% and 6.6 in inflection, respectively). In spite of this, the obtained electron density map had good enough quality to interpret the structure (Figure 3B). Dichromatic X-rays can be used for saving total experimental time and the total cost of beam time.

Conclusion

The MAD method is widely used as an experimental phasing method in modern protein crystallography. We have proposed the trichromatic concept, which optimizes MAD experiments by synchrotron radiation. The trichromatic concept has been applied to MAD analyses of many proteins successfully. In these experiments, we have collected many MAD data sets, including various anomalous specimens (zinc [14–16], selenium [17, 18], platinum [19, 20], gold [21], mercury [22–24], lead [25], etc.), and successfully achieved straightforward structure determination. In conclusion, the trichromatic concept is well suited for the de novo crystallographic analysis of proteins, and the trichromator is advantageous in synchrotron protein crystallography.

Experimental Procedures

The experimental steps of trichromatic data collection are summarized in Figure 1B. The first gap of the undulator is set to emit the absorption edge energy of an anomalous scatterer and the other is set to emit the remote energy for the control data. The three wavelengths are selected by inspecting the X-ray absorption near edge spectrum (XANES) prior to data collection.

In the conventional MAD data collection method, data collection is performed serially with different wavelengths. On the other hand, in the trichromatic MAD method, data collection is performed serially with different oscillation angles by rapidly switching wavelengths. One characteristic parameter available in the trichromator operation is the number of images to be collected without switching wavelengths. For example, if the parameter is set at five, the wavelength is switched over after exposing five frames. This parameter was set at one in all of following trichromatic data collections to minimize the time lag error in dispersive terms. However, recent MAD experiments were often performed in between the two modes: the wavelength is changed after collecting a few frames at one wavelength.

The comparison between the trichromatic method and the conventional method was examined with identical crystals and the same beamline configuration. The crystals of selenomethionyl chitosanase (ChoA) from *Matsuebacter chitosanotabidus* 3001 (mw = 34,000, $P2_12_12_1$, a = 51.5, b = 56.2, c = 206.8 Å, Z = 4, Z_{Se} = 54) took the shape of a bar with dimensions of 0.02 × 0.02 × 0.3 mm [17]. Cho1 and -2 data sets were collected with the trichromatic and conventional methods, respectively. To be identical with respect to crystal conditions, the two sets were collected from different parts of an identical crystal. Incident wavelengths were selected with λ_{Peak} = 0.97905, $\lambda_{Inflection}$ = 0.97960, λ_{Remote} = 1.02000 Å from the selenium XANES profile of the crystal.

The dichromatic diffraction measurement was examined with the crystal of zinc-dependent β-carbonic anhydrase (CA) from the red alga *Porphyridium purpureum* ($P2_1$, a = 63.4, b = 112.8, c = 73.2 Å, β = 103.6°) [14]. The fluorescence spectrum from the zinc atom was measured to select the wavelengths (λ_{Peak} = 1.2823, $\lambda_{Inflection}$ = 1.2825, λ_{Remote} = 1.0200 Å). The MAD data collection was performed with dichromatic diffraction of the inflection and remote wavelengths and with monochromatic diffraction of the peak wavelength. The two and one wavelengths were iteratively introduced to the specimen.

All of the data set was collected at 90 K with imaging plate detectors, R-AXIS IV or V, and independently processed and scaled to

merge with the HKL suite [26]. The experimental MAD phase was calculated with CCP4 (MLPHARE) [13] and/or SOLVE [12].

Acknowledgments

In the construction of the beamline, much helpful cooperation and advice were received from T. Ishikawa and the SPring-8 project team. Y. Inoue and the RIKEN synchrotron structural biology research group supports and encourages beamline construction and research studies. K. Hamada (Shimane University), T. Tsukihara (Osaka University), I. Yamaguchi (RIKEN), and colleagues were favored to protein samples for the evaluation of the trichromatic concept. We are also grateful to our colleagues M. Miyano, H. Motoshima, M. Sugahara, H. Ago, G. Ueno, M. Kimura, and M. Furuichi for valuable discussions.

Received: February 14, 2002
Revised: May 29, 2002
Accepted: June 14, 2002

References

1. Ueki, T., and Yamamoto, M. (1999). The start of a new generation: the present status of the SPring-8 synchrotron and its use in structural biology. Structure *7*, R183–R187.
2. Hendrickson, W.A. (1999). Maturation of MAD phasing for the determination of macromolecular structures. J. Synchr. Rad. *6*, 845–851.
3. Hendrickson, W.A. (1991). Determination of macromolecular structures from anomalous diffraction of synchrotron radiation. Science *254*, 51–58.
4. Hendrickson, W.A., and Ogata, C.M. (1997). Phase determination from multiwavelength anomalous diffraction measurements. Methods Enzymol. *276*, 494–523.
5. Hendrickson, W.A., Horton, J.R., and LeMaster, D.M. (1990). Selenomethionyl proteins produced for analysis by multiwavelength anomalous diffraction (MAD): a vehicle for direct determination of three-dimensional structure. EMBO J. *9*, 1665–1672.
6. Nave, C. (1995). Radiation damage in protein crystallography. Rad. Phys. Chem. *45*, 483–490.
7. Gonzalez, A., and Nave, C. (1994). Radiation damage in protein crystals at low temperature. Acta Crystallogr. D *50*, 874–877.
8. Yamamoto, M., Fujisawa, T., Nakasako, M., Tanaka, T., Uruga, T., Kimura, H.,Yamaoka, H., Inoue, Y., Iwasaki, H., Ishikawa, T., et al. (1994). Conceptual design of SPring-8 contract beamline for structural biology. Rev. Sci. Instrum. *66*, 1833–1835.
9. Tanaka, T., Marechal, X.M., Hara, T., Tanabe, T., and Kitamura, H. (1998). Construction of a vertical undulator at SPring-8. J. Synchr. Rad. *5*, 414–416.
10. Yamamoto, M., Kumasaka, T., Fujisawa, T., and Ueki, T. (1998). Trichromatic concept at SPring-8 RIKEN beamline I. J. Synchr. Rad. *5*, 222–225.
11. Yamamoto, M., Kumasaka, T., Yamazaki, H., Sasaki, K., Yokozawa, Y., and Ishikawa, T. (2001). Development of high-speed imaging plate detector. Nucleic Instr. Methods A *467–468*, 1160–1162.
12. Terwilliger, T.C., and Berendzen, J. (1999). Automated structure solution for MIR and MAD. Acta Crystallogr. D *55*, 849–861.
13. CCP4 (Collaborative Computational Project 4) (1994). The CCP4 suite: programs for protein crystallography. Acta Crystallogr. D *50*, 760–763.
14. Mitsuhashi, S., Mizushima, T., Yamashita, E., Yamamoto, M., Kumasaka, T., Moriyama, H., Ueki, T., Miyachi, S., and Tsukihara, T. (2000). X-ray structure of β-carbonic anhydrase from the red alga, *Porphyridium purpureum*, reveals a novel catalytic site for CO_2 hydration. J. Biol. Chem. *275*, 5521–5526.
15. Nakasako, M., Kimura, M., and Yamaguchi, I. (1999). Crystallization and preliminary X-ray diffraction studies of blasticidin S deaminase from *Aspergillus terreus*. Acta Crystallogr. D *54*, 547–548.
16. Sugahara, M., Mikawa, T., Kumasaka, T., Yamamoto, M., Kato, R., Fukuyama, K., Inoue, Y., and Kuramitsu, S. (2000). Crystal structure of a repair enzyme of oxidatively damaged DNA, MutM (Fpg), from an extreme thermophile, *Thermus thermophilus* HB8. EMBO J. *19*, 3857–3869.
17. Park, J.K., Shimono, K., Ochiai, N., Shigeru, K., Kurita, M., Ohta, Y., Tanaka, K., Matsuda, H., and Kawamukai, M. (1999). Purification, characterization, and gene analysis of a chitosanase (ChoA) from *Matsuebacter chitosanotabidus* 3001. J. Bacteriol. *181*, 6642–6649.
18. Lee, S.J., Imamoto, N., Sakai, H., Nakagawa, A., Kose, S., Koike, M., Yamamoto, M., Kumasaka, T., Yoneda, Y., and Tsukihara, T. (2000). The adoption of a twisted structure of importin-β is essential for the protein-protein interaction required for nuclear transport. J. Mol. Biol. *302*, 251–264.
19. Toyoda, T., Tin, O.F., Ito, K., Fujiwara, T., Kumasaka, T., Yamamoto, M., Garber, M.B., and Nakamura, Y. (2000). Crystal structure combined with genetic analysis of the *Thermus thermophilus* ribosome recycling factor shows that a flexible hinge may act as a functional switch. RNA *6*, 1432–1444.
20. Kunishima, N., Shimada, Y., Tsuji, Y., Sato, T., Yamamoto, M., Kumasaka, T., Nakanishi, S., Jingami, H., and Morikawa, K. (2000). Structural bases of glutamate recognition by a dimeric metabotropic glutamate receptor. Nature *407*, 971–997.
21. Tahirov, T.H., Inoue-Bungo, T., Morii, H., Fujikawa, A., Sasaki, M., Kimura, K., Shiina, M., Sato, K., Kumasaka, T., Yamamoto, M., et al. (2001). Structural analyses of DNA recognition by the AML1/Runx-1 Runt domain and its allosteric control by CBF-β. Cell *104*, 755–767.
22. Nakai, T., Hasegawa, T., Yamashita, E., Yamamoto, M., Kumasaka, T., Ueki, T., Nanba, H., Ikenaka, Y., Takahashi, S., Sato, M., and Tsukihara, T. (2000). Crystal structure of N-carbamyl-D-amino acid amidohydrolase with a novel catalytic framework common to amidohydrolases. Structure *8*, 729–737.
23. Palczewski, K., Kumasaka, T., Hori, T., Behnke, C.A., Motoshima, H., Fox, B.A., Le Trong, I., Teller, D.C., Okada, T., Stenkamp, R.E., et al. (2000). Crystal structure of rhodopsin: a G protein-coupled receptor. Science *289*, 739–745.
24. Samatey, F.A., Imada, K., Nagashima, S., Vonderviszt, F., Kumasaka, T., Yamamoto, M., and Namba, K. (2001). Structure of the bacterial flagellar protofilament and implications for a switch for supercoiling. Nature *410*, 331–337.
25. Motoshima, H., Inagaki, K., Kumasaka, T., Furuichi, M., Inoue, H., Tamura, T., Esaki, N., Soda, K., Tanaka, N., Yamamoto, M., and Tanaka, H. (2000). Crystal structure of the pyridoxal-5′-phosphate dependent L-methionine γ-lyase from *Pseudomonas putida*. J. Biochem. (Tokyo) *128*, 349–354.
26. Otwinowski, Z., and Minor, W. (1997). Processing of X-ray diffraction data collected in oscillation mode. Methods Enzymol. *276*, 307–326.
27. McRee, D.E. (1999). XtalView/Xfit—a versatile program for manipulating atomic coordinates and electron density. J. Struct. Biol. *125*, 156–165.
28. Merrit, E.A., and Murphy, M.E.P. (1992). Raster3D version 2.0. A program for photorealistic molecular graphics. Acta Crystallogr. D *50*, 869–873.
29. Roussel, A., and Cambillau, C. (1989). Silicon Graphics Geometry Partners Directory (Mountain View, CA: Silicon Graphics), pp. 77–79.